Topics in Catalysis
https://doi.org/10.1007/s11244-021-01415-2

ORIGINAL PAPER

Structure Sensitivity and Hydration Effects in Pt/TiO_2 and Pt/TiO_2–SiO_2 Catalysts for NO and Propane Oxidation

Sara Viéitez-Calo[1] · David J. Morgan[1] · Stan Golunski[1] · Stuart H. Taylor[1] · Martyn V. Twigg[2]

Accepted: 30 January 2021

Abstract
The NO and propane oxidation activities of a series of 1%Pt/TiO_2–SiO_2 catalysts show different underlying trends as the support composition changes. Surface characterisation of the catalysts indicates that the trend for NO conversion is consistent with the oxidation rate being dependent on the degree of metallic character of the Pt nanoparticles, rather than their morphology. Although a similar correlation is expected for the total oxidation of propane, it is masked by the effects of adventitious ions originating during manufacture of the support materials. When residual chloride is present in the support, most of the exposed Pt is stabilised in its low-activity ionic form; while support materials containing W or oxidised-S ions give rise to catalysts with much higher activity than expected from their measured Pt^0 content. When a Cl-containing, but SiO_2-free, TiO_2 support material is pre-treated hydrothermally, the propane-oxidation activity of the resultant Pt/TiO_2 catalyst is substantially improved, so that it matches the performance of highly-metallic Pt supported on TiO_2 containing 16 wt% SiO_2. The hydrothermal pre-treatment removes residual chloride from the support material, but it also leaves the catalyst in a hydrated state. We show that, by controlling the metallic content of Pt nanoparticles, understanding the promoting and inhibiting effects of adventitious ions, and optimising the degree of catalyst hydration, the activity of 1%Pt/TiO_2–SiO_2 catalysts can be made to exceed that of a benchmark 2%Pt/γ-Al_2O_3 formulation for both NO and propane oxidation.

Keywords NO oxidation · Propane oxidation · Platinum · TiO_2–SiO_2 · Adventitious ions · Catalyst hydration

1 Introduction

Among the key functions of a diesel oxidation catalyst is its ability to convert both alkanes and NO [1–3]. The deep oxidation of alkanes allows hydrocarbon emission standards (e.g. [4] in EU) to be met by current diesel vehicles [5] and off-road machinery [6]. Although the conversion of NO to NO_2 can be a pivotal step in the passive oxidation of soot particulate in catalysed filters and during NO_x adsorption catalysis, its most important role currently is to optimise the rate of selective catalytic reduction of NO_x [7, 8]. This dual alkane/NO functionality can be achieved, together with the other less demanding oxidation reactions of CO and alkenes, by using a relatively high loading of Pt or a Pt-rich bimetallic combination of Pt and Pd (typically 2–2.5% Pt by weight of the monolith washcoat) supported on γ-Al_2O_3 [9, 10].

TiO_2 is a potential alternative to γ-Al_2O_3 as a support material for Pt-based oxidation catalysts [11]. It interacts strongly with platinum group metals, stabilising the metal nanoparticles against sintering, while also conferring chemical resistance and sulphur-tolerance to the catalysts [12]. Although commercial TiO_2 support materials (which are often bi-phasic mixtures of anatase and rutile [13]) have a moderate surface area, this can be increased and made thermally stable by the inclusion of SiO_2 [14]. As SiO_2 interacts very weakly with platinum group metals [15], its main role is thought to be in the control of the surface morphology of the TiO_2 [16], through which it can influence the dispersion [15] and oxidation state [17] of the Pt, as well as the extent of the interface between Pt nano-particles and the TiO_2 present in the support [18].

Here we show that, apart from increasing the surface area, the presence of SiO_2 in a TiO_2 support material can influence the surface Pt^{2+}/Pt^0 ratio of the supported platinum,

✉ Stan Golunski
segolunski@gmail.com

[1] Cardiff Catalysis Institute, School of Chemistry, Cardiff University, Cardiff CF10 3AT, UK

[2] Twigg Scientific and Technical Limited, Caxton, Cambridge CB23 3PQ, UK

Published online: 11 February 2021

which is in effect a measure of exposed Pt^0. The NO-oxidation activity in the kinetic regime, i.e. below the temperature at which the reaction becomes equilibrium limited (typically ~ 350 °C), shows an inverse correlation with the Pt^{2+}/Pt^0 ratio, except when chloride is present. By contrast, deep oxidation of propane does not show this same simple dependence on the proportion of metallic Pt present at the surface. Instead, it is highly sensitive to the presence of Cl, W and oxidised-S ions, which can originate during the manufacture of the support materials. We also show that hydrothermal pre-treatment of a Cl-containing TiO_2 support material not only removes the adventitious ions, but results in the formation of a hydrated catalyst with high propane oxidation activity. In practical terms, knowledge of these effects enables the Pt loading to be reduced in catalysts used for both NO and alkane oxidation.

2 Experimental

2.1 Catalyst Preparation

Proprietary support materials were sourced from two different specialist suppliers (TiO_2 and TiO_2 with 5 and 16 wt% SiO_2 from one supplier; TiO_2 and TiO_2 with 10 wt% SiO_2 from another supplier), which made it essential to start by comparing their bulk structures and surface compositions. Characterisation of the crystalline phases by X-ray diffraction (see below) showed that, depending on the source, each material contained either anatase alone or a mixture of anatase and rutile. A series of catalysts with 1wt% loading of Pt was prepared by impregnating these support materials with a non-aqueous solution of a chloride-free precursor: '$Pt(acac)_2$' (Pt(II)2,4-pentanedionate, Alfa Aesar) dissolved in toluene (Fisher, HPLC grade). The suspensions were stirred for 24 h at room temperature. After removing the solvent in a rotary evaporator, the residue was dried at 100 °C for 16 h and calcined at 400 °C for 5 h under static air. Additionally, two benchmark catalysts were prepared using the same impregnation method to support 1 wt% or 2 wt% platinum on anhydrous γ-Al_2O_3 (Merck Performance Materials).

Hydrated variants of the TiO_2-containing catalysts were prepared by hydrothermally pre-treating the support materials. In *simple hydration*, suspensions were formed by adding deionised water (100 cm^3) to the support materials (4 g); while in *basic hydration*, aqueous NH_4OH (1 mol dm^{-3}; 100 cm^3) was added to the support materials (4 g) to form suspensions with a pH of 11–12. The suspensions were heated at ≈ 110 °C under reflux for 24 h, before the solids were isolated (by filtration) and dried (16 h at ≈ 70 °C). The resulting hydrated materials were then impregnated with platinum precursor, dried and calcined following the method described above.

2.2 Catalyst Notation

Our notation indicates the wt% loading of Pt in the catalysts and of any SiO_2 present in the support materials. For example, 1%Pt/TiO_2–10%SiO_2 represents a catalyst in which 1% by weight is Pt, with the Pt supported on a material that contains 90 wt% TiO_2 and 10 wt% SiO_2. We use the term *as-prepared* to emphasise that a catalyst has not undergone any further treatment (e.g. reduction) following calcination, and to distinguish it from the hydrated variants.

2.3 Characterisation

The specific surface area of the support materials and catalysts was measured on a Micromeritics Gemini 2360 analyser coupled with a Micromeritics FlowPrep 060. A five-point BET method was used, in which nitrogen was adsorbed at − 196 °C, over the standard pressure range 0.05–0.35 p/p_0. Before the measurements were made, the samples were outgassed by exposure to N_2 at 120 °C for 45 min.

Pulsed chemisorption of CO was carried out in a flow of He, using a Quantachrome ChemBET TPR/TPD analyser, with the intention of estimating the platinum dispersion in the catalysts. Samples were pre-treated under pure H_2 at 300 °C for 2 h, at a flow rate of 30 cm^3 min^{-1}. This pre-treatment was expected to reduce any ionic species on the surface of the Pt nanoparticles formed during preparation of the catalysts, without changing the size or morphology of the nanoparticles. The apparent dispersion values were calculated from the total CO uptake at 30 °C, based on the assumption of 1:1 stoichiometry between adsorbed CO molecules and the number of exposed Pt surface atoms.

Powder X-ray diffraction (XRD) patterns were obtained on a PANanalytical X'Pert Pro diffractometer using a Cu Kα X-ray source operating at 40 kV and 40 mA. The signal was recorded for 2θ values between 10° and 80° at increments of 0.02°. The bulk components of the catalytic materials were identified by matching the diffraction patterns with standards in the JCPDS database.

X-ray photoelectron spectroscopy (XPS) analysis of the samples was carried out on a Kratos Axis Ultra DKD photoelectron spectrometer with a monochromatic Al source (1486.6 eV). All spectra were obtained at a pass energy of 40 eV for high resolution scans and 160 eV for survey spectra, over an analysis area of 700 × 300 μm^2. The measured binding energies were normalised with respect to the C (1s) peak of the surface adventitious carbon (284.7 eV). Qualitative and quantitative interpretation of the data was carried out using CasaXPS software.

Scanning electron microscopy (SEM) images were obtained using a Carl Zeiss EVO 40 microscope operated at 25 kV. Samples were mounted on carbon Leit adhesive discs. Images were collected using backscattered and secondary electron detectors. For analysis by EDX (X-ray energy dispersive spectroscopy), high probe currents (up to 25 nA) were required to allow sufficient generation of X-rays. The data were collected using an Oxford EDX analyser coupled to the microscope.

Surface examination by high resolution transmission electron microscopy (HRTEM) was carried out on a JEOL-2100 JEM microscope, at an accelerating voltage of 300 kV. The samples were dispersed in ethanol and dropped on a copper mesh with a carbon micro-grid. STEM-EDX spectrum imaging experiments were performed on the same instrument.

Data from diffuse reflectance infrared spectroscopy (DRIFTS) were collected on a Bruker Tensor 27 spectrometer fitted with a liquid N_2-cooled mercury cadmium telluride detector. Samples were placed within a 'praying mantis' high-temperature diffuse reflection environmental reaction chamber (HVC-DRP-4) fitted with zinc selenide windows. Prior to analysis, the samples (as-supplied and hydrated support materials) were ground to a fine powder using an agate mortar and pestle. For background scans, finely ground KBr was used. Spectra were recorded from 64 scans across the frequency range of 600–4000 cm^{-1}.

2.4 Catalyst testing

Catalyst testing was carried out in a stainless steel fixed-bed reactor (internal diameter: 0.5 cm), which was heated in a horizontal tube furnace. The typical catalyst charge was 30 mg of powdered material (particle size: 250–300 μm), packed between two plugs of quartz wool. When assessing alkane-oxidation activity, the gas-feed (flow rate: 200 cm^3 min^{-1}; GHSV: 50,000 h^{-1}) contained 0.5% propane in synthetic air (20% O_2 / 80% He), so that the C_3H_8:O_2 ratio was strongly fuel-lean. The reactants and products were analysed by online gas chromatography, using a Varian 3800 gas chromatograph fitted with two columns (HayeSep Q to separate CO_2 and hydrocarbons; molecular sieve 13X to separate CO, O_2 and N_2) and with thermal conductivity and flame ionisation detectors. The propane conversion and associated carbon balance were measured at catalyst bed temperatures between 100 and 550 °C, at 50 °C intervals. Several measurements were taken to ensure stable conversion had been reached at each temperature.

For NO-oxidation testing, the gas-feed was substituted by 1000 ppm NO in an oxidising atmosphere (7.5% O_2, He balance), such that the NO:O_2 ratio was 1:75 by volume. The gas composition exiting the reactor was analysed continuously by an FT-IR spectrometer (Gasmet DX-4000) with an integrated 400 cm^3 heated analysis cell. Concentration measurements (in vol-ppm) were calculated using Calcmet™ software with internal calibration standards.

3 Results and Discussion

3.1 Characterisation and Evidence of Metal-Support Interactions

Bulk characterisation by X-ray diffraction (Fig. 1) showed that the support materials in the series TiO_2(bi-phasic), TiO_2–5%SiO_2 and TiO_2–16%SiO_2 contained mixtures of anatase (≈80%) and rutile (≈20%); whereas TiO_2 (anatase-only) and TiO_2–10%SiO_2, which were both from a different source, contained anatase as the only crystalline phase. The BET surface area measurements were higher when SiO_2 was present and, as expected [18, 19], each value decreased (by 1–10%) after deposition of the platinum (Table 1). 1%Pt/TiO_2–10%SiO_2, in which the support was comprised of only one crystalline phase (anatase), had the highest surface area (96 m^2 g^{-1}); 1%Pt/TiO_2 (bi-phasic), which was made from SiO_2-free bi-phasic TiO_2 had the lowest surface area (50 m^2 g^{-1}).

The CO chemisorption values for the catalysts decreased (from a maximum of 0.24 μmol g^{-1} for 1%Pt on bi-phasic TiO_2) as the proportion of SiO_2 in the support material increased, becoming negligible when the support material contained 16% SiO_2 (Table 1). For catalysts in which there is a weak interaction between the metal nanoparticles and the support material, such a trend would indicate a marked decrease in Pt dispersion (i.e. the Pt nanoparticles become larger) as the SiO_2 content increases. However, as discussed below, this effect on dispersion was not confirmed

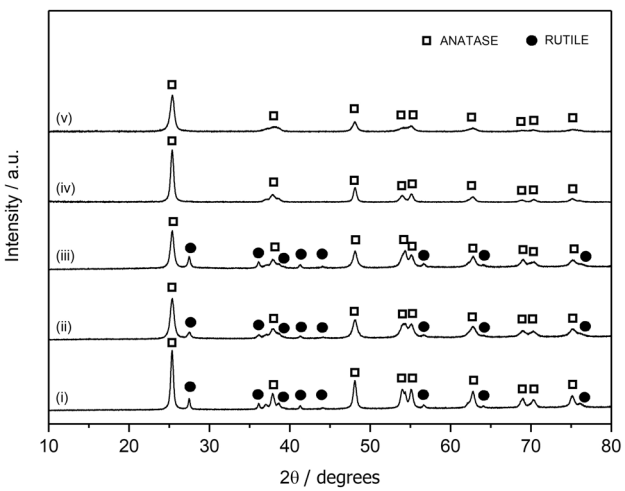

Fig. 1 XRD of catalyst support materials: (i) bi-phasic TiO_2, (ii) TiO_2–5%SiO_2, (iii) TiO_2–16%SiO_2, (iv) anatase-only TiO_2, (v) TiO_2–10%SiO_2

Table 1 Textural characterisation of support materials and as-prepared catalysts (*NA* indicates negligible adsorption). Any adventitious elements detected on the surface are also shown

Sample	BET surface area ($m^2\ g^{-1}$)	CO chemisorption ($\mu mol\ g^{-1}$)	Adventitious element: atomic%
Bi-phasic TiO_2	52	NA	Cl: 0.2
1% Pt/TiO_2(bi-phasic)	50	0.24	Cl: 0.2
Anatase-only TiO_2	80	NA	S: 0.8
1%Pt/TiO_2(anatase-only)	75	0.13	S: 0.7
TiO_2–5%SiO_2	84	NA	None
1% Pt/TiO_2–5%SiO_2	83	0.08	None
TiO_2–10%SiO_2	107	NA	W: 1.6
1% Pt/TiO_2–10%SiO_2	96	0.06	W: 1.5
TiO_2–16%SiO_2	72	NA	None
1% Pt/TiO_2–16%SiO_2	71	NA	None

by electron microscopy. Instead, the trend is consistent with a strong metal-support interaction (SMSI) induced by reduction, resulting in a thin but impervious overlayer of reduced metal oxide forming on the metal nanoparticles, which blocks CO chemisorption. Although, in this study, the reduction temperature (300 °C) prior to chemisorption was lower than that used by Tauster et al. (500 °C) in their classic work on the induction of SMSI in Pt/TiO_2 [20], it has been shown that the presence of SiO_2 can promote SMSI by segregating TiO_2 into nano-domains that interact strongly with Pt nanoparticles [16]. As pointed out by Spencer [21], the threshold temperature for SMSI is not determined by thermodynamic equilibrium, but is dependent on the rate of surface diffusion of Ti–O species, which in turn will depend on the extent of contact between TiO_2 and Pt.

XPS survey spectra indicated the presence of adventitious elements (in their ionic form) on the surface of some of the support materials, which persisted even after Pt was added by impregnation to form the catalysts (Table 1). It is likely that these elements originated during manufacture of the support materials, and hence we deduce that the anatase-only TiO_2 (which contained oxidised S) had been made from the mineral source by a traditional sulphate route [22], whereas the bi-phasic TiO_2 (which contained Cl) had been made *via* $TiCl_4$ [23]; we suspect that the TiO_2–10%SiO_2 (which contained W) had been made in a plant used to produce WO_3–TiO_2 catalysts for selective catalytic reduction of NO_x [24].

From the region for Pt 4f in the high resolution XPS scans (Fig. 2), the spectra could be fitted with two pairs of overlapping Lorentzian curves. The Pt $4f_{7/2}$ and Pt $4f_{5/2}$ lines at 71.4 eV and 74.7 eV are attributed to metallic platinum (Pt^0), while the second pair at 72.9 eV and 76.3 eV can be assigned to platinum oxide (PtO). The relative peak areas indicate that the atomic proportion of metallic platinum at the surface increased from 23% in Pt/TiO_2(bi-phasic) to 80% in Pt/TiO_2–16%SiO_2. These results could be indicating the stabilisation of larger metallic nanoparticles when SiO_2 is present in the support material. However, HRTEM analysis of multiple areas of the surface of Pt/TiO_2–5%SiO_2 and Pt/TiO_2–16%SiO_2 (Fig. 3a and b) showed that the typical Pt particle size was between 1.5 and 5 nm in both catalysts. By contrast, small metal nanoparticles were difficult to find on SiO_2-free Pt/TiO_2 by HRTEM, but larger particles (≈10 nm) could be identified from STEM images and EDX analysis (Fig. 3c). The results show that inclusion of SiO_2 in a TiO_2 support material increases the Pt dispersion, but the size of the Pt nanoparticles does not then greatly change as a function of SiO_2 content.

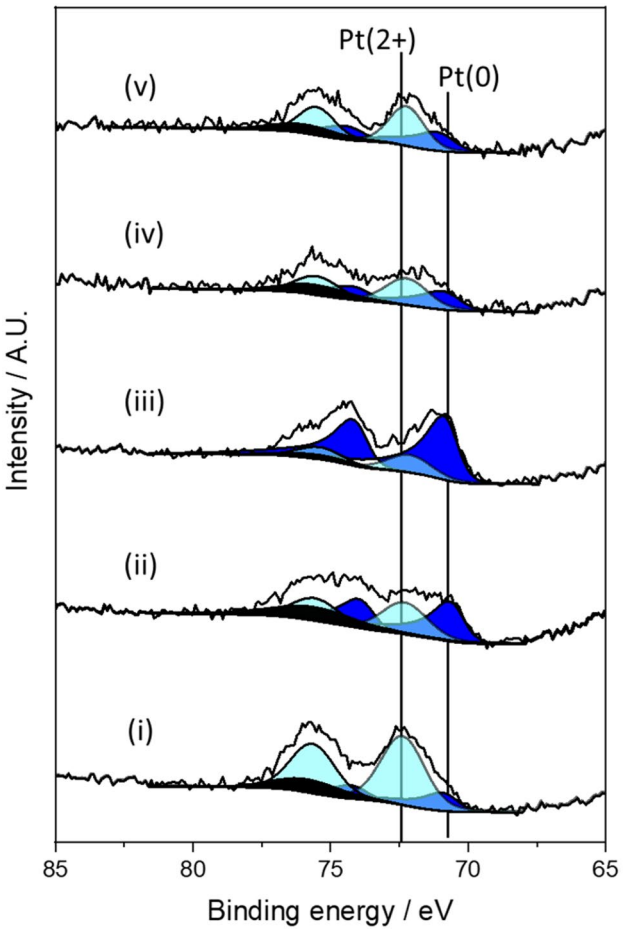

Fig. 2 XPS spectra of as-prepared catalysts, showing the Pt 4f binding energy regions: (i) 1%Pt/TiO_2(bi-phasic), (ii) 1%Pt/TiO_2–5%SiO_2, (iii) 1%Pt/TiO_2–16%SiO_2, (iv) 1%Pt/TiO_2(anatase-only), (v) 1%Pt/TiO_2–10%SiO_2

3.2 NO Oxidation

The NO-oxidation performance of each of the catalysts gave rise to a characteristic bell-shaped plot for

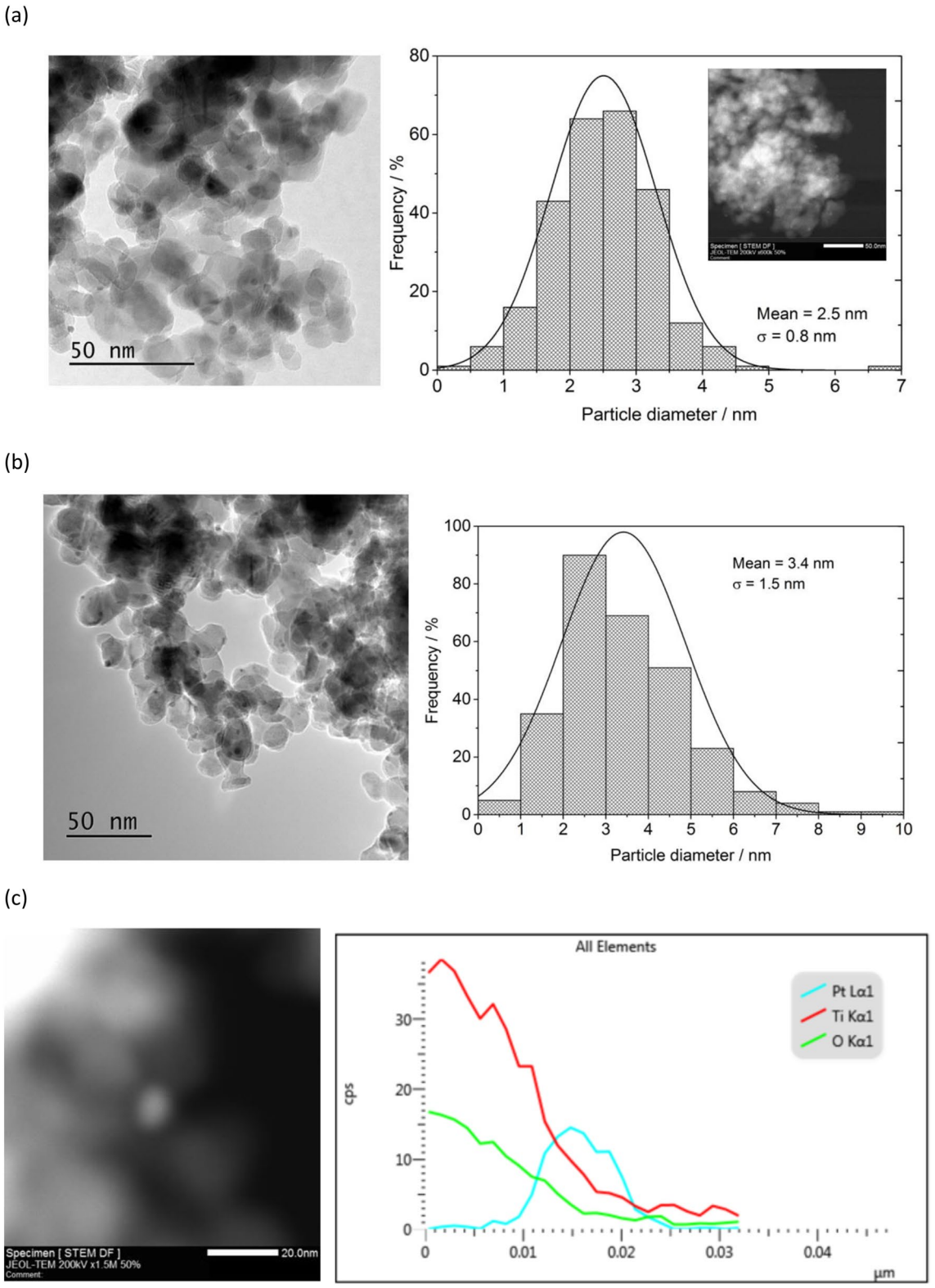

Fig. 3 Electron microscopy of as-prepared catalysts. **a** HRTEM image and particle size analysis of 1%Pt/TiO_2–5%SiO_2; **b** HRTEM image and particle size analysis of 1%Pt/TiO_2–16%SiO_2; **c** STEM image and EDX analysis of 1%Pt/TiO_2 (bi-phasic)

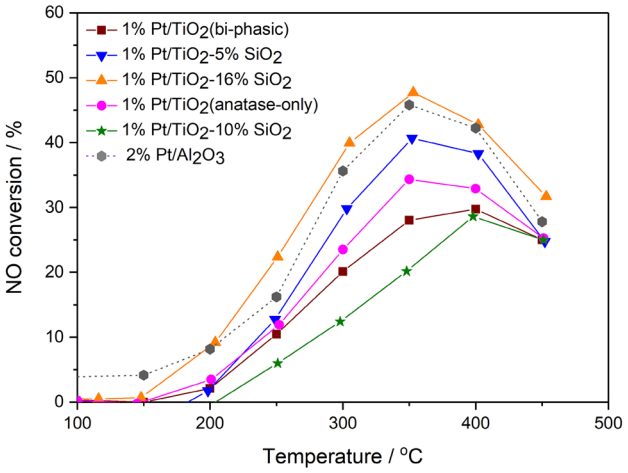

Fig. 4 NO-oxidation activity of as-prepared catalysts as a function of temperature

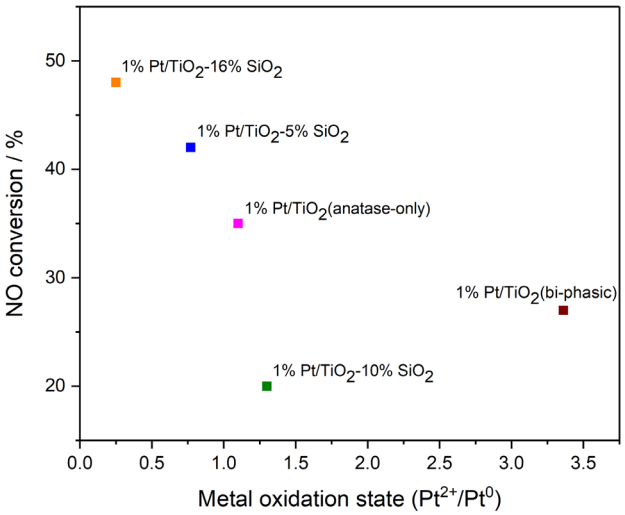

Fig. 5 NO-oxidation activity at 350 °C of as-prepared catalysts as a function of mean oxidation state of surface Pt

NO conversion to NO_2 (Fig. 4), reflecting kinetic limitations at temperatures below ca. 350 °C and thermodynamic equilibrium limitations at higher temperatures [25, 26]. The most active catalyst (1%Pt/TiO_2–16%SiO_2) closely matched the performance of the benchmark 2%Pt/Al_2O_3, including achieving near-equilibrium yields of NO_2 at temperatures above 350 °C. However, within the SiO_2-containing series, the intrinsic activities did not correlate simply with SiO_2 content, as seen from the relative activities within the kinetically-limited temperature range, which followed the order: 1%Pt/TiO_2–10%SiO_2 < 1%Pt/TiO_2(bi-phasic) < 1%Pt/TiO_2(anatase-only) < 1%Pt/TiO_2–5%SiO_2 < 2%Pt/γ-Al_2O_3 < 1%Pt/TiO_2–16%SiO_2.

It was also apparent that the intrinsic activity was not primarily influenced by the anatase/rutile ratio (compare the activity plots in Fig. 4 for 1%Pt supported on anatase-only and the bi-phasic supports), the BET surface area (see values listed in Table 1) or the Pt particle size (see HRTEM and STEM data in Fig. 3). It did, however, show a dependence on the mean oxidation state of the surface platinum. With the exception of 1%Pt/TiO_2(bi-phasic), which contained adventitious Cl, there was a near-linear inverse correlation between NO conversion (at 350 °C) and Pt^{2+}/Pt^0 ratio (Fig. 5). This is consistent with the active sites for NO oxidation being exposed metal atoms at the surface of the platinum nanoparticles [27–29]. However, our results appear to conflict with the classic work by Ross and co-workers [30] on structure sensitivity of Pt/SiO_2 and Pt/Al_2O_3 catalysts, which showed that the specific-activity for NO oxidation is influenced by the size of the Pt nanoparticles (with larger Pt nanoparticles resulting in higher specific-activity). The model proposed by Olsson and Fridell [31] allows our observations to be reconciled with those of Ross and co-workers [30]. In the Olsson–Fridell model, NO-oxidation activity primarily depends on the metallic character of the Pt nanoparticles, which in turn may depend on the size of the nanoparticles (e.g. when the support is SiO_2 or Al_2O_3, as used by Ross and co-workers [30].)

The outlier in Fig. 5, 1%Pt/TiO_2(bi-phasic), had the highest Pt^{2+}/Pt^0 ratio (3.36) and hence the lowest surface concentration of metallic platinum, and yet its activity exceeded that of 1%Pt/TiO_2–10%SiO_2 ($Pt^{2+}/Pt^0 = 1.3$). Our surface characterisation of 1%Pt/TiO_2(bi-phasic) suggests that the adventitious Cl^- from the support material had stabilised most of the platinum in its ionic form, with the small proportion of Pt^0 forming relatively large particles (≈ 10 nm). Although there is scant literature on the effects of chloride on NO oxidation over Pt catalysts, work on NOx reduction by hydrocarbons [32] indicates that Cl^- ions inhibit dissociation of chemisorbed NO on Pt. The relatively high NO-oxidation activity that we observe for 1%Pt/TiO_2(bi-phasic), despite the predominance of Pt^{2+} at the surface, may reflect the role of Cl^- ions in preventing active sites on the Pt becoming blocked by dissociated NO.

3.3 Propane oxidation

Propane is not a typical component of exhaust gas from an internal combustion engine, but as one of the most difficult alkanes to oxidise completely [33], it is often used to assess the ability of potential aftertreatment catalysts to eliminate the alkane component of hydrocarbon emissions. The propane oxidation activity of the SiO_2-containing 1%Pt/TiO_2 catalysts gave rise to a succession of light-off curves, all of which were shifted to lower temperatures relative to the trace for 1%Pt supported on bi-phasic TiO_2 (Fig. 6).

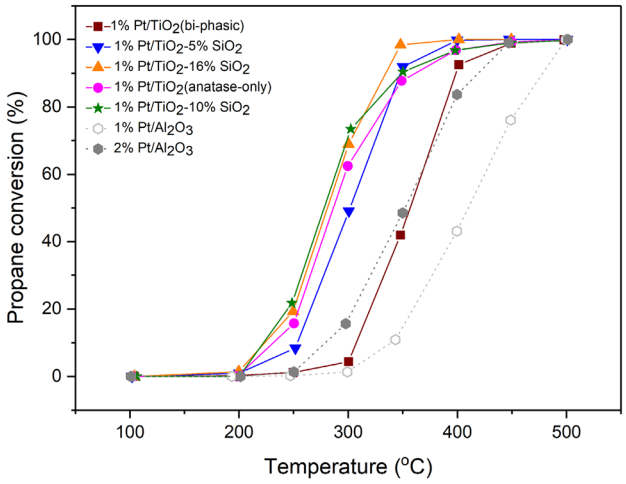

Fig. 6 Propane-oxidation activity of as-prepared catalysts as a function of temperature

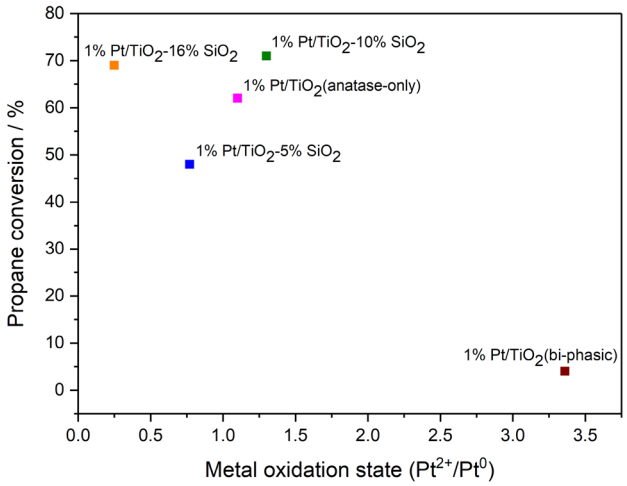

Fig. 7 Propane-oxidation activity of as-prepared catalysts at 300 °C as a function of mean oxidation state of surface Pt

The relative activities of the complete set of catalysts, including the two Pt/Al_2O_3 benchmark catalysts, adopted the following order (where T_{10} and T_{50} indicate the temperatures for 10% and 50% propane conversion):

$1\%Pt/Al_2O_3$ [$T_{10}=340$ °C, $T_{50}=410$ °C] < $1\%Pt/TiO_2$(bi-phasic) [$T_{10}=310$ °C, $T_{50}=355$ °C] < $2\%Pt/Al_2O_3$ [$T_{10}=280$ °C, $T_{50}=350$ °C] < $1\%Pt/TiO_2$-5% SiO_2 [$T_{10}=250$ °C, $T_{50}=300$ °C] < $1\%Pt/TiO_2$(anatase-only) [$T_{10}=235$ °C, $T_{50}=290$ °C] < 1% Pt/TiO_2-16% SiO_2 [$T_{10}=225$ °C, $T_{50}=278$ °C] < 1% Pt/TiO_2-10% SiO_2 [$T_{10}=225$ °C, $T_{50}=275$ °C].

In light of published data [34] which show that the crystal form of TiO_2 does not have a marked effect on the VOC oxidation activity of Pt/TiO_2, it was surprising that $1\%Pt/TiO_2$(anatase-only) was much more active than $1\%Pt/TiO_2$(bi-phasic). It is also notable that the activity of each of the SiO_2-containing catalysts was substantially greater than that of $2\%Pt/Al_2O_3$, despite having only 50% of the platinum loading.

When compared to NO oxidation (Fig. 5), the propane-oxidation activity of the TiO_2-containing catalysts did not show a similar dependence on the mean oxidation state of the surface platinum (Fig. 7). Furthermore, although the presence of SiO_2 in the TiO_2 support material altered the textural properties of the catalysts, the changes in propane-oxidation activity could not be accounted for simply in terms of an increase in BET surface area (see Supplementary Information Fig. 1) or by changes in Pt particle size. The most likely explanation for the non-linearity observed in Fig. 7 is that the activity was being affected by the adventitious ions present in three of the catalysts (Table 1), i.e. Cl in $1\%Pt/TiO_2$(bi-phasic), S in $1\%Pt/TiO_2$(anatase-only) and W in $1\%Pt/TiO_2$–$10\%SiO_2$. It is known that propane oxidation over Pt catalysts is promoted by oxidised sulphur species [35–37] and by WO_3 [34, 38], but inhibited by chloride ions [39, 40].

Significantly, the propane oxidation performance of the least active catalyst ($1\%Pt$ on bi-phasic TiO_2) could be promoted to the level of the catalyst with the highest SiO_2 content ($1\%Pt/TiO_2$–$16\%SiO_2$) by subjecting the TiO_2 to basic hydration before impregnation with Pt (Fig. 8). Even simple hydration of the bi-phasic TiO_2 improved the activity of the resultant catalyst (Fig. 8).

Both simple and basic hydration of the bi-phasic TiO_2 increased its bulk density by > 50%, but did not measurably alter either its bulk phase composition or its surface area (see Supplementary Information Table 2; Fig. 2). The most

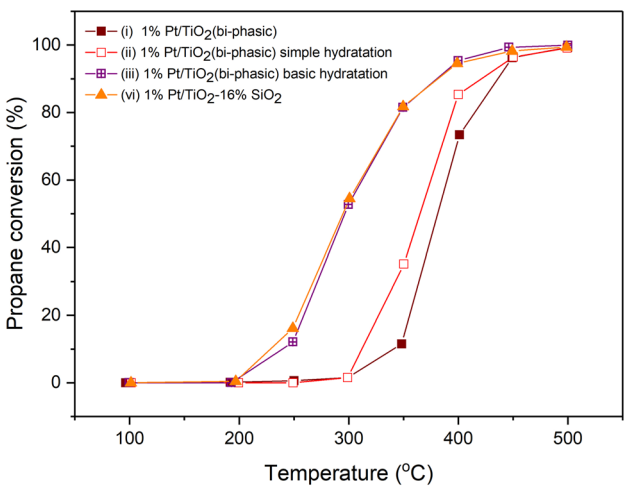

Fig. 8 Propane-oxidation activity as a function of temperature of as-prepared $1\%Pt/TiO_2$(bi-phasic), $1\%Pt/TiO_2$ after simple hydration of the support material and $1\%Pt/TiO_2$(bi-phasic) after basic hydration of the support material. Compared to as-prepared $1\%Pt/TiO_2$–$16\%SiO_2$

obvious change was the absence of the chloride signal during XPS analysis of the hydrated materials, indicating that the adventitious Cl^- ions had been removed by the hydrothermal pre-treatment. However, another perceptible change became apparent from characterisation by DRIFTS, but this was not in the regions of the spectrum where we were expecting so see the effects of chloride displacement by hydroxyl species on the surface of TiO_2 [41], namely between 3640 and 2500 cm^{-1} (O–H stretching vibrations) and at 1630 cm^{-1} (O–H bending). As can be seen in Fig. 9, the spectrum for the highly active variant of 1%Pt/TiO_2(bi-phasic), formed following basic hydration of the support, showed the appearance of a small but broad peak at 1450 cm^{-1}. This peak was also present in the spectrum of the highly active SiO_2-free catalyst in which 1%Pt was supported on anatase-only TiO_2, but not in the spectrum of a high SiO_2-content catalyst (Fig. 9iii). Although the other peaks at lower wavenumbers (1050−800 cm^{-1}) can be assigned to the vibration modes for Ti–O–Ti [41–43], the peak at 1450 cm^{-1} is not readily recognisable from published data for TiO_2. However, a similar feature, which has been detected at 1449 cm^{-1} by in-situ FTIR of Pt/Al_2O_3 during propane and O_2 co-adsorption [38], has been attributed to the surface water that forms as the propane oxidises [38].

Overall, these results showed that a highly active propane-oxidation catalyst, with equivalent performance to a catalyst with high SiO_2 content, could be prepared from SiO_2-free TiO_2 by subjecting it to hydrothermal pre-treatment. In addition to removing chloride ions from the catalyst surface, the effect of the pre-treatment was to alter the state of hydration of the TiO_2 in the support,

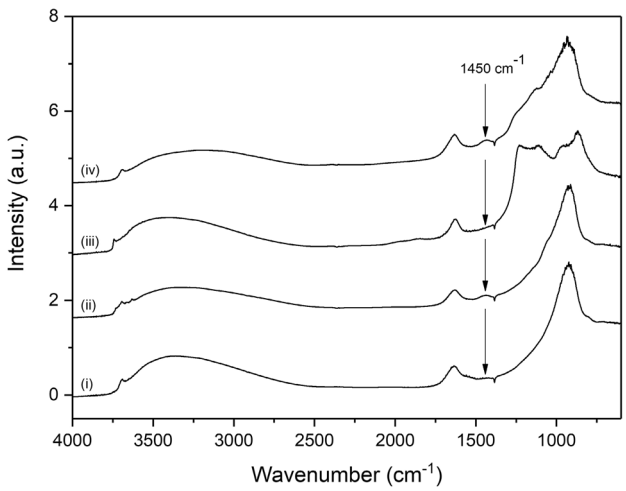

Fig. 9 DRIFTS analysis of support materials, showing the position of the peak at 1450 cm^{-1} that acts as a diagnostic of the hydrated state: (i) as-supplied bi-phasic TiO_2, (ii) bi-phasic TiO_2 after basic hydration, (iii) as-supplied TiO_2-16%SiO_2, (iv) as-supplied anatase-only TiO_2

which appears to be a key parameter in determining the intrinsic activity of Pt catalysts for the deep oxidation of alkanes. In light of the work of Caporali et al. [44], which showed that H_2O-derived oxygen was active in the deep oxidation of hydrocarbons over a Pd diesel oxidation catalyst, we propose that hydration of TiO_2 provides a similar hydroxyl-mediated pathway to CO_2, in addition to the reaction between adsorbed alkane and dissociated O_2 on Pt^0 active sites. One of the limitations of our study, however, is that it did not allow us to determine the relative extent to which propane oxidation over 1%Pt on bi-phasic TiO_2 is enhanced by (i) removal of the chloride ions, compared to (ii) increasing the degree of hydration, both of which occur during hydrothermal pre-treatment.

4 Conclusions

In this study, oxidation catalysts comprising 1%Pt supported on TiO_2 and TiO_2–SiO_2 were prepared from a chloride-free Pt precursor using a non-aqueous impregnation method, so eliminating the metal precursor as a source of any adventitious chloride ions in the catalysts. Characterisation of these catalysts was complicated by the well-known SMSI effect in Pt/TiO_2 [20], the onset of which is known to be enhanced by the presence of SiO_2 in the support material [16]. The resultant suppression of CO-chemisorption gave rise to anomalously large values for the estimated Pt crystallite size with increasing SiO_2 content, whereas electron microscopy showed that, in fact, relatively small nanoparticles (typically 2–5 nm diameter) were being stabilised by the silica.

The NO oxidation activity of the catalysts showed an inverse dependence on the mean oxidation state of the exposed Pt. This is consistent with the accepted model of structure-sensitivity for NO oxidation over Pt [31], in which a higher specific rate of reaction results from a greater number of Pt^0 surface sites (usually associated with larger metal nanoparticles [32]), whereas more ionic nanoparticles (which are often smaller) are less active. As the oxidation of alkanes is known to exhibit the same type of structure-sensitivity [45], in which the Pt oxidation state [46, 47] rather than its morphology is the determining factor, a similar inverse correlation would be expected between propane-oxidation activity and the Pt^{2+}/Pt^0 ratio. However, we have observed that the correlation breaks down when other factors exert an influence, including the presence of adventitious ions (which can arise from the routes taken during manufacture of the support materials) and the state of hydration of the catalysts.

Supplementary Information The online version contains supplementary material available at https://doi.org/10.1007/s11244-021-01415-2.

Acknowledgements The authors gratefully acknowledge funding provided by Cardiff University. SG thanks Dr Timothy Watling (Johnson Matthey Technology Centre) for advice on structure sensitivity in automotive catalysis.

Compliance with Ethical Standards

Conflict of interest The authors have no conflicts of interest to declare that are relevant to the content of this article.

References

1. Lambert CK (2019) Current state of the art and future needs for automotive exhaust catalysis. Nat Catal 2:554–557
2. Russell A, Epling WS (2011) Diesel oxidation catalysts. Catal Rev Sci Eng 53:337–423
3. York APE, Tsolakis A (2010) Cleaner vehicle emissions. Encyclopedia of materials: science and technology, 2nd edn. Elsevier, North Holland, pp 1–7
4. Regulation No 83 of UNECE - the United Nations Economic Commission for Europe (2019) Uniform provisions concerning the approval of vehicles with regard to the emission of pollutants according to engine fuel requirements. Off J Eur Union L45:1–243
5. Twigg MV (2011) Catalytic control of emissions from cars. Catal Today 163:33–41
6. Dou D (2012) Application of diesel oxidation catalyst and diesel particulate filter for diesel engine powered non-road machines. Platinum Metals Rev 56:144–154
7. Granger P (2017) Challenges and breakthroughs in post-combustion catalysis: how to match future stringent regulations. Catal Sci Technol 7:5195–5211
8. Dhal GC, Mohan D, Prasad R (2017) Preparation and application of effective different catalysts for simultaneous control of diesel soot and NO_x emissions: an overview. Catal Sci Technol 7:1803–1825
9. Majewski WA (2018) DOC applications. In: DieselNet Technology Guide. Revision 2018.05, dieselnet.com
10. Ahmadinejad M, Etheridge JE, Watling TC, Johansson Å, John G (2015) Computer simulation of automotive emission control systems. Johnson Matthey Technol Rev 59:152–165
11. Bagheri S, Julkapli NM, Hamid SBA (2014) Titanium dioxide as a catalyst support in heterogeneous catalysis. Sci World J 727496:1–21
12. Escandón LS, Ordóñez S, Díez FV (2008) Sulphur poisoning of palladium catalysts used for methane combustion: effect of the support. J Hazard Mater 153:742–750
13. Ohtani B, Prieto-Mahaney OO, Li D, Abe R (2010) What is Degussa (Evonik) P25? Crystalline composition analysis, reconstruction from isolated pure particles and photocatalytic activity test. J Photochemistry Photobiology A 216:179–182
14. Bonne M, Pronier S, Can F, Courtois X, Valange S, Tatibouët J-M, Royer S, Marécot P, Duprez D (2010) Synthesis and characterization of high surface area TiO_2/SiO_2 mesostructured nanocomposite. Solid State Sci 12:1002–1012
15. Min BK, Santra AK, Goodman DW (2003) Understanding silica-supported metal catalysts: Pd/silica as a case study. Catal Today 85:113–124
16. Bonne M, Samoila P, Ekou T, Especel C, Epron F, Marécot P, Royer S, Duprez D (2010) Control of titania nanodomain size as a route to modulate SMSI effect in Pt/TiO_2 catalysts. Catal Commun 12:86–91
17. Kim M-Y, Choi J-S, Toops T, Jeong E-S, Han SW, Schwartz V, Chen J (2013) Coating SiO_2 support with TiO_2 or ZrO_2 and effects on structure and CO oxidation performance of Pt catalysts. Catalysts 3:88–103
18. Yoshida H, Yazawa Y, Hattori T (2003) Effects of support and additive on oxidation state and activity of Pt catalyst in propane combustion. Catal Today 87:19–28
19. Avila MS, Vignatti CI, Apesteguía CR, Garetto TF (2014) Effect of support on the deep oxidation of propane and propylene on Pt-based catalysts. Chem Eng J 241:52–59
20. Tauster SJ, Fung SC, Garten RL (1978) Strong metal-support interactions: group 8 noble metals supported on titanium dioxide. J Am Chem Soc 100:170–175
21. Spencer MS (1985) Models of strong metal-support interaction (SMSI) in Pt on TiO_2 catalysts. J Catal 93:216–223
22. Gázquez MJ, Bolívar JP, Garcia-Tenorio R, Vaca F (2014) A review of the production cycle of titanium dioxide pigment. Mater Sci Appl 5:441–458
23. Braun JH, Baidins A, Marganski RE (1992) TiO_2 pigment technology: a review. Prog Org Coat 20:105–138
24. He Y, Ford ME, Zhu M, Liu Q, Wu Z, Wachs IE (2016) Selective catalytic reduction of NO by NH_3 with WO_3-TiO_2 catalysts: influence of catalyst synthesis method. Appl Catal B 188:123–133
25. Olsson L, Westerberg B, Persson H, Fridell E, Skoglundh M, Andersson B (1999) A kinetic study of oxygen adsorption/desorption and NO oxidation over Pt/Al_2O_3 catalysts. J Phys Chem B 103:10433–10439
26. Hong Z, Wang Z, Li X (2017) Catalytic oxidation of nitric oxide (NO) over different catalysts: an overview. Catal Sci Technol 7:3440–3452
27. Després J, Elsener M, Koebel M, Kröcher O, Schnyder B, Wokaun A (2004) Catalytic oxidation of nitrogen monoxide over Pt/SiO_2. Appl Catal B: Environ 50:73–82
28. Mulla SS, Chen N, Cumaranatunge L, Blau GE, Zemlyanov DY, Delgass WN, Epling WS, Ribeiro FH (2006) Reaction of NO and O_2 to NO_2 on Pt: kinetics and catalyst deactivation. J Catal 241:389–399
29. Bhatia D, McCabe RW, Harold MP, Balakotaiah V (2009) Experimental and kinetic study of NO oxidation on model Pt catalysts. J Catal 266:106–119
30. Xue E, Seshan K, Ross JRH (1996) Roles of supports, Pt loading and Pt dispersion in the oxidation of NO to NO_2 and of SO_2 to SO_3. Appl Catal B 11:65–79
31. Olsson L, Fridell E (2002) The influence of Pt oxide formation and Pt dispersion on the reactions $NO_2 \Leftrightarrow NO + 1/2\ O_2$ over Pt/Al_2O_3 and $Pt/BaO/Al_2O_3$. J Catal 210:340–353
32. Yentekakis IV, Lambert RM, Konsolakis M, Kallithrakas-Kontos N (2002) On the effects of residual chloride and of barium promotion on Pt/γ-Al_2O_3 catalysts in the reduction of NO by propene. Catal Lett 81:181–185
33. Choudhary TV, Banerjee S, Choudhary VR (2002) Catalysts for combustion of methane and lower alkanes. Appl Catal A 234:1–23

34. Papaefthimiou P, Ioannides T, Verykios XE (1998) Performance of doped Pt/TiO, (W6+) catalysts for combustion of volatile organic compounds (VOCs). Appl Catal B 15:75–92
35. Ansell GP, Golunski SE, Hatcher HA, Rajaram RR (1991) Effects of SO_2 on the alkane activity of three-way catalysts. Catal Lett 11:183–190
36. Burch R, Crittle DJ, Hayes MJ (1999) C-H bond activation in hydrocarbon oxidation on heterogeneous catalysts. Catal Today 47:229–234
37. Lee AF, Wilson K, Lambert RM, Hubbard CP, Hurley RG, McCabe RW, Gandhi HS (1999) The origin of SO_2 promotion of propane oxidation over Pt/Al_2O_3 catalysts. J Catal 184:491–498
38. Pereira da Silva MA, Cardoso RM, Schmal M (2003) Propane oxidation on $Pt\text{-}WO_3/\gamma\text{-}Al_2O_3$ systems. Braz J Chem Eng 20:51–56
39. Marecot P, Fakche A, Kellali B, Mabilon G, Prigent M, Barbier J (1994) Propane and propene oxidation over platinum and palladium on alumina: effects of chloride and water. Appl Catal B 3:283–294
40. Argyle MD, Bartholomew CH (2015) Heterogeneous catalyst deactivation and regeneration: a review. Catalysts 5:145–269
41. Arun Kumar D, Merline Shyla J, Xavier FP (2012) Synthesis and characterization of TiO_2/SiO_2 nano composites for solar cell applications. Appl Nanosci 2:429–436
42. Zhang X, Zhang F, Chan K-Y (2005) Synthesis of titania–silica mixed oxide mesoporous materials, characterization and photocatalytic properties. Appl Catal A: Gen 284:193–198
43. Kemdeo SM, Sapkal VS, Chaudhari GN (2010) TiO_2–SiO_2 mixed oxide supported MoO_3 catalyst: physicochemical characterization and activities in nitration of phenol. J Mol Cat A: Chem 323:70–77
44. Caporali R, Chansai S, Burch R, Delgado JJ, Goguet A, Hardacre C, Mantarosie L, Thompsett D (2014) Critical role of water in the direct oxidation of CO and hydrocarbons in diesel exhaust after treatment catalysis. Appl Catal B 147:764–769
45. Garetto TF, Apesteguía CR (2000) Oxidative catalytic removal of hydrocarbons over Pt/Al_2O_3. Catal Today 62:189–199
46. Kobayashi M, Morita A, Ikeda M (2007) The support effect in oxidizing atmosphere on propane combustion over platinum supported on TiO_2, TiO_2–SiO_2 and TiO_2–SiO_2–WO_3. Appl Catal B 71:94–100
47. Yazawa Y, Yoshida H, Hattori T (2002) The support effect on platinum catalyst under oxidizing atmosphere: improvement in the oxidation-resistance of platinum by the electrophilic property of support materials. Appl Catal A 237:139–148